PERGAMON

International Journal of Multiphase Flow 26 (2000) 421–433

International Journal of Multiphase Flow

www.elsevier.com/locate/ijmulflow

Lattice-Boltzmann simulations of fluidization of rectangular particles

Dewei Qi

Department of Paper and Printing Science and Engineering, Western Michigan University, Kalamazoo, MI 49008, USA

Received 13 August 1998; received in revised form 15 March 1999

Abstract

Lattice-Boltzmann simulations on fluidization of two-dimensional rectangular multi-particles falling against gravity are performed. The particle behavior is dominated by inertia effects associated with wakes. The long bodies of the rectangular particles turn horizontal dominantly. Relative stable particle clusters and inverted T clusters are found. Drafting, kissing and melting can be used to characterize the behavior of multi-rectangular particles. Simulation results are well consistent with the experimental results of three-dimensional cylindric and disk particles.

1. Introduction

Fluidization of solid particles is an important subject in a variety of industries. For example, wood fibers have to be fluidized to have an uniform structure before entering the forming section of a paper machine. Understanding of essential mechanism of aggregation and dispersion of particles will benefit process design of chemical engineering.

Some investigators have reported their works on sedimentation of spherical, and non-spherical particles. The formation of natural clusters of particles were reported. Evidence of the importance of aggregates formed from drafting, kissing and tumbling in both low and high Reynolds number was given by Happel and Pfeffer (1960), Joseph et al. (1987), and Feng et al. (1994a). Joseph group conducted the first experimental fluidization of non-spherical particles.

E-mail address: dewei.qi@wmich.edu (D. Qi).

0301-9322/00/$ - see front matter
PII: S0301-9322(99)00017-8

Cylinders and disks were used in their experiments. The non-spherical particle behavior is quit different from spherical particles. They found that long bodies of particles are perpendicular to the stream lines of flows and oscillate around the horizontal position. The high pressure at the points of stagnation gives rise to a couple causing the body to turn broadside on. There are very strong wakes behind fluidized cylinders. Other particles may be sucked into the wakes. Joseph et al. (1987) reported that inverted 'T' clusters and other type clusters may be formed by two or more particles. These clusters formed by multi-particles are relatively stable. Much more information can be found in the article by Joseph et al. (1987).

Lattice-Boltzmann (LB) simulations on fluidization of two-dimensional (2D) rectangular multi-particles falling against gravity are performed in this work. The purpose is to demonstrate that the LB method has a capacity to handle non-spherical multi-particles correctly.

2. Lattice-Boltzmann simulation

The method of LB simulation (Wolfram, 1986; D'Humieres et al., 1986; D'Humieres and Lallemand, 1987; Frich et al., 1987; McNamara and Zanetti, 1988; Qian et al., 1992; Dahlburg et al., 1987) of suspensions has been developed to simulate the complex shape particles (Ladd, 1994a, 1994b; Koch and Ladd, 1997; Aidun and Lu, 1995; Aidun and Qi, 1998; Aidun et al., 1998; Qi, 1997a, 1997b, 1999a, 1999b). The simulation domain is divided into a discrete lattice. A distribution function of fluid density in the lattice node is used to represent the real flows. A two speed model of LB simulation is used, and the vectors $\mathbf{e}_{\sigma i}$ representing both lattice spacing and fluid velocities in the model are listed in Table 1 for the 2D case. The LB equation with a single relaxation time is given by

$$f_{\sigma i}(\mathbf{x}+\epsilon\mathbf{e}_{\sigma i},t+\epsilon)-f_{\sigma i}(\mathbf{x},t)=-\frac{1}{\tau}\Big[f_{\sigma i}(\mathbf{x},t)-f^{(0)}_{\sigma i}(\mathbf{x},t)\Big], \tag{1}$$

where $f_{\sigma i}(\mathbf{x},t)$ is the fluid particle distribution function, $f^{(0)}_{\sigma i}(\mathbf{x},t)$ is the equilibrium distribution function, τ is the single relaxation time, and ϵ is the small lattice time unit in physical unit. The kinematic viscosity ν is related to τ by $\nu=(2\tau-1)/6$. In the simulations, $f^{(0)}_{\sigma i}(\mathbf{x},t)$ is taken as

Table 1
Velocity vector for cubic lattice in the two-dimensional case

σ	i	$\mathbf{e}_{\sigma ix}$	$\mathbf{e}_{\sigma iy}$	$\mathbf{e}_{\sigma i}$
1	1	1	0	1
1	2	−1	0	1
1	3	0	1	1
1	4	0	−1	1
2	1	1	1	$\sqrt{2}$
2	2	−1	−1	$\sqrt{2}$
2	3	−1	1	$\sqrt{2}$
2	4	1	−1	$\sqrt{2}$

$$f_{\sigma i}^{(0)}(\mathbf{x},t) = A_\sigma + B_\sigma(\mathbf{e}_{\sigma i}\cdot\mathbf{u}) + C_\sigma(\mathbf{e}_{\sigma i}\cdot\mathbf{u})^2 + D_\sigma u^2, \tag{2}$$

where $\sigma = 1$ corresponds to the fluid particles moving to the near-neighbors along axial directions; $\sigma = 2$ corresponds to the fluid particles moving to their second near-neighbors along diagonal directions; $\sigma = 0$ and $i = 0$ correspond to the rest fluid particles; $\mathbf{u}$ is the mean velocity of fluid particles at a node.

To derive the Navier–Stokes equations, the Chapman–Nskog procedure (Liboff, 1990) is utilized, and a long-wavelength, low-frequency approximation and a multi-scaling analysis are adopted (Hou, 1995). Thus,

$$\frac{\partial}{\partial t} = \epsilon\frac{\partial}{\partial t_1} + \epsilon^2\frac{\partial}{\partial t_2} + \cdots \tag{3}$$

and

$$\frac{\partial}{\partial x} = \epsilon\frac{\partial}{\partial x}, \tag{4}$$

where t_1 and t_2 represent fast and slow time scales, respectively. The distribution function is also expanded as

$$f_{\sigma i} = f_{\sigma i}^{(0)} + \epsilon f_{\sigma i}^{(1)} + \epsilon^2 f_{\sigma i}^{(2)}, \tag{5}$$

where the zeroth-order term is the equilibrium distribution function. Since the mass, and momentum are conserved in collisions at each node:

$$\rho(\mathbf{x},t) = \sum_{\sigma i} f_{\sigma i}(\mathbf{x},t) = \sum_{\sigma i} f_{\sigma i}^{(0)}, \tag{6}$$

$$\rho(\mathbf{x},t)\mathbf{u} = \sum_{\sigma i} f_{\sigma i}(\mathbf{x},t)\mathbf{e}_{\sigma i} = \sum_{\sigma i} f_{\sigma i}^{(0)}(\mathbf{x},t)\mathbf{e}_{\sigma i}, \tag{7}$$

the summations over non-equilibrium density are zero: $\sum_{\sigma i} f_{\sigma i}^{(l)} = 0$ and $\sum_{\sigma i} f_{\sigma i}^{(l)}\mathbf{e}_{\sigma i} = 0$ for $l > 0$. Substituting the above expansions into Eq. (1), the equations of first and second order in ϵ are obtained and written as

$$\frac{\partial}{\partial t_1} f_{\sigma i}^{(0)} + \mathbf{e}_{\sigma i}\cdot\nabla_1 f_{\sigma i}^{(0)} = -\frac{1}{\tau} f_{\sigma i}^{(1)}, \tag{8}$$

and

$$\frac{\partial}{\partial t_2} f_{\sigma i}^{(0)} + \left(\frac{\partial}{\partial t_1} + \mathbf{e}_{\sigma i}\cdot\nabla\right)\left(1 - \frac{1}{2\tau}\right) f_{\sigma i}^{(1)} = -\frac{1}{\tau} f_{\sigma i}^{(2)}. \tag{9}$$

When Eq. (8) is summed over σ and i, the mass conservation equation is obtained as

$$\frac{\partial \rho}{\partial t} = \nabla\rho\mathbf{u} \tag{10}$$

The momentum equation is obtained by multiplying Eq. (9) by $\mathbf{e}_{\sigma i}$ and then summing over all directions:

$$\frac{\partial \rho \mathbf{u}}{\partial t} + \nabla \cdot \mathbf{\Pi}^{(0)} + \left(1 - \frac{1}{2\tau}\right)\mathbf{\Pi}^{(1)} = 0, \tag{11}$$

where $\mathbf{\Pi}^{(0)}$ and $\mathbf{\Pi}^{(1)}$ are the momentum flux tensors,

$$\mathbf{\Pi}^{(0)} = \sum_{\sigma i} \mathbf{e}_{\sigma i}\mathbf{e}_{\sigma i} f^{(0)}_{\sigma i}, \tag{12}$$

and

$$\mathbf{\Pi}^{(1)} = \sum_{\sigma i} \mathbf{e}_{\sigma i}\mathbf{e}_{\sigma i} f^{(1)}_{\sigma i} \tag{13}$$

Constitutive relations for the tensors are obtained by matching moments of the distribution function with the terms in the Navier–Stokes equations. After manipulating algebra, the Navier–Stokes equations are recovered, and the suitable coefficients in the fluid density distribution function are found for two-dimensional

$$A_1 = \frac{1}{9}\rho, \quad B_1 = \frac{1}{3}\rho, \quad C_1 = \frac{1}{2}\rho,$$

$$D_1 = -\frac{1}{6}\rho, \quad A_2 = \frac{1}{72}\rho, \quad B_2 = \frac{1}{24}\rho,$$

$$C_2 = \frac{1}{16}\rho, \quad D_2 = -\frac{1}{48}\rho, \quad A_0 = \frac{2}{9}\rho,$$

$$D_0 = -\frac{1}{6}\rho \tag{14}$$

In order to match the fluid velocity with the velocity of solid in the solid–fluid interface, Ladd proposed a collision rule which is given by

$$f_{\sigma i'}(\mathbf{x}, t+1) = f_{\sigma i}(\mathbf{x}, t_+) - 2B_\sigma(\mathbf{e}_{\sigma i} \cdot \mathbf{U}_b), \tag{15}$$

where $\mathbf{x}$ is the position of the node adjacent to the solid-surface with velocity $\mathbf{U}_b$, t_+ is the post collision time which is the same as the definition by Ladd (1994a), i' denotes the reflected direction, and i the incident direction. The above rule is applied to the boundary nodes in both sides of the solid-surface. As a result, a no-slip boundary condition for moving solid particles is imposed by the collision rule in such a way that the fluid mass is conserved at each time step by allowing exchange of population of fluid at the boundary nodes adjacent to both sides of the solid-surface. The hydrodynamic force exerted on the solid particle at the boundary node is

$$F\left(\mathbf{x}+\frac{1}{2}\mathbf{e}_{\sigma i}\right)=2\mathbf{e}_{\sigma i}\left(f_{\sigma i}(\mathbf{x},t_{+})-B_{\sigma}(\mathbf{U}_{b}\cdot\mathbf{e}_{\sigma i})\right) \tag{16}$$

where $\mathbf{U}_b=\mathbf{U}_0+\mathbf{\Omega}\times\mathbf{x}_b$; $\mathbf{U}_0$ is the velocity of the center of mass; $\mathbf{U}_b$ is the velocity of solid–fluid interface at the node; $\mathbf{\Omega}$ is the angular velocity of the solid particle; $\mathbf{x}_b=\mathbf{x}+\frac{1}{2}\mathbf{e}_{\sigma i}-\mathbf{R}$; $\mathbf{R}$ is the center of the corresponding solid particle. The total force F_{T} and torques T_{T} on the solid particles are obtained by

$$F_{\mathrm{T}}=\sum F\left(\mathbf{x}+\frac{1}{2}\mathbf{e}_{\sigma i}\right) \tag{17}$$

$$T_{\mathrm{T}}=\sum\left(\mathbf{x}+\frac{1}{2}\mathbf{e}_{\sigma i}-\mathbf{R}\right)\times F\left(\mathrm{x}+\frac{1}{2}\mathrm{e}_{\sigma i}\right) \tag{18}$$

The summation is over all the boundary nodes in the fluid region associated with a particular solid particle.

In the LB method, the nodes are fixed and the solid particles move over on the (nodes) grids. Whenever a node crosses the fluid–solid interface and enters the solid region, the momentum of the flow at the boundary node may exert a force on the solid particle. The force F_I (Aidun et al., 1998; Qi, 1999a) at the node is

$$F_I(\mathbf{x},t)=\rho(\mathbf{x},t)\mathbf{u}(\mathbf{x},t) \tag{19}$$

where ρ is the density of the fluid at the node. Similarly, whenever a node crosses the solid–fluid interface and leave the solid region. The flow in the node should add a force F_O on the solid particle, i.e.

$$F_O(\mathbf{x},t)=-\rho(\mathbf{x},t)\mathbf{u}(\mathbf{x},t) \tag{20}$$

It is important that the approach still allows fluid to enter the inside of solid to conserve total mass of fluid at each time step. First, conservation of fluid mass guarantees the recovery of the Navier–Stokes equations from LB method. Otherwise, the Navier–Stokes equations would not be recovered.

Both the translations and rotations of each particle are updated at each Newtonian dynamic time step by using a so-called 'velocity-Verlet' scheme (Swope et al., 1982). The scheme is written as

$$\mathbf{R}(t+\delta t)=\mathbf{R}(t)+\delta t\mathbf{U}_0(t)+\frac{1}{2}\delta t^2\mathbf{F}(t)/M \tag{21}$$

$$\mathbf{U}_0(t+\delta t)=\mathbf{U}_0(t)+\frac{1}{2}\delta t\mathbf{F}(t)/M+\mathbf{F}(t+\delta t)/M \tag{22}$$

where $\mathbf{R}$ is the position of the mass center of a solid particle, $\mathbf{F}$ is the total force on the solid particle, M is the mass of the solid particle.

The reliability of the LB simulation of suspensions at finite Reynolds numbers has been

evaluated and confirmed by comparing LB simulation results with both finite-element and experimental results (Qi, 1999).

3. Fluidization of rectangular particles

Two-dimensional rectangular particles may have a similar behavior to three-dimensional (3D) disk or cylindric particles. Before simulating them in a 3D space, as first step, conducting a simulation in a 2D space is a cheaper way to gain an insight into a physical picture of multi-particle interaction.

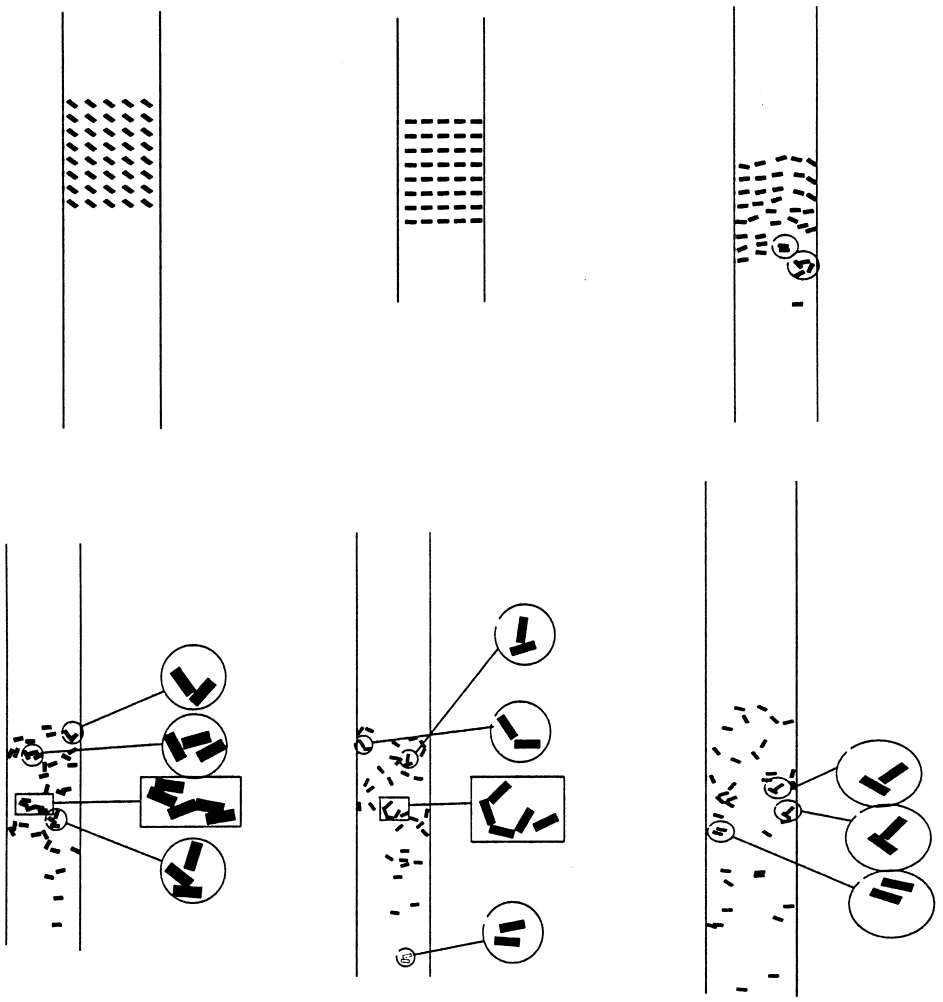

Fig. 1. Snap shots of rectangular particles at $t = 0$, 2600, 18,200, 25,600, 35,000, 40,000. The inverted T formed by two particles, stable doublets, triplets, and large clusters formed by an array of a few rectangles floating broadside on are shown.

4. Simulation

Two rectangular particles have been simulated by Qi (1999a). The same method is extended to deal with multi-rectangular particles. The length l of rectangular particle is 30 and the width $w = 10$. Forty such rectangular particles are initially located in a regular order in a 2D channel and the titling angles of the long axis of all the rectangles with the horizontal direction are set to 135° as shown in Fig. 1. The density ratio of the solid particles to fluid is 2. They settle down under gravity. The fluid velocity at the bottom boundary is set to zero and the boundary is always 325 away from the bottom particle. The gradient of the fluid velocity in the vertical direction at the top boundary is set to zero and the boundary is always kept 325 distance from the top particle. Therefore, the simulation box is expanded in the gravity direction during simulation due to relative movement among the particles and the boundary conditions used in this work. The initial simulation box size is 261×1000 and the size at $t = 50{,}000$ is 261×1963.

4.1. Angular ordering

The snapshots of particle configurations at different time in the simulations are shown in

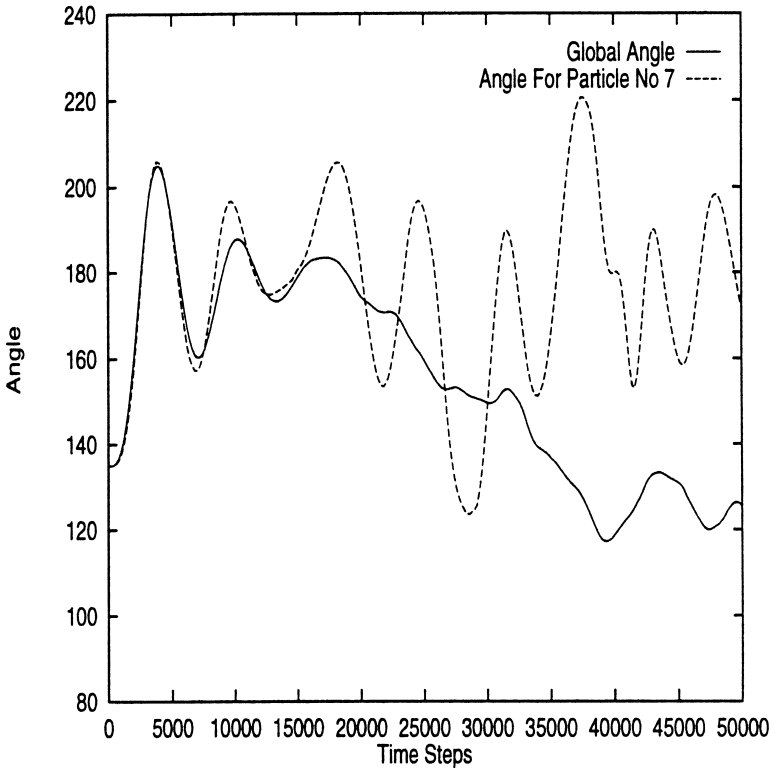

Fig. 2. Rotational angles.

Fig. 1. The diagrams from the left to the right and from the top to the bottom in the figure correspond to a time order of $t = 0$, 2600, 18,200, 25,600, 30,000 and 40,000. The global averages of tilting angle as a function of time are shown in Fig. 2.

The particles turn horizontal collectively after 2600 time steps, and slowly and collectively oscillate around 180° like a 'whole body'.The particles start to melt from the 'whole body' around time step $t = 18{,}000$. Since the distance of the most left particles from the left wall is

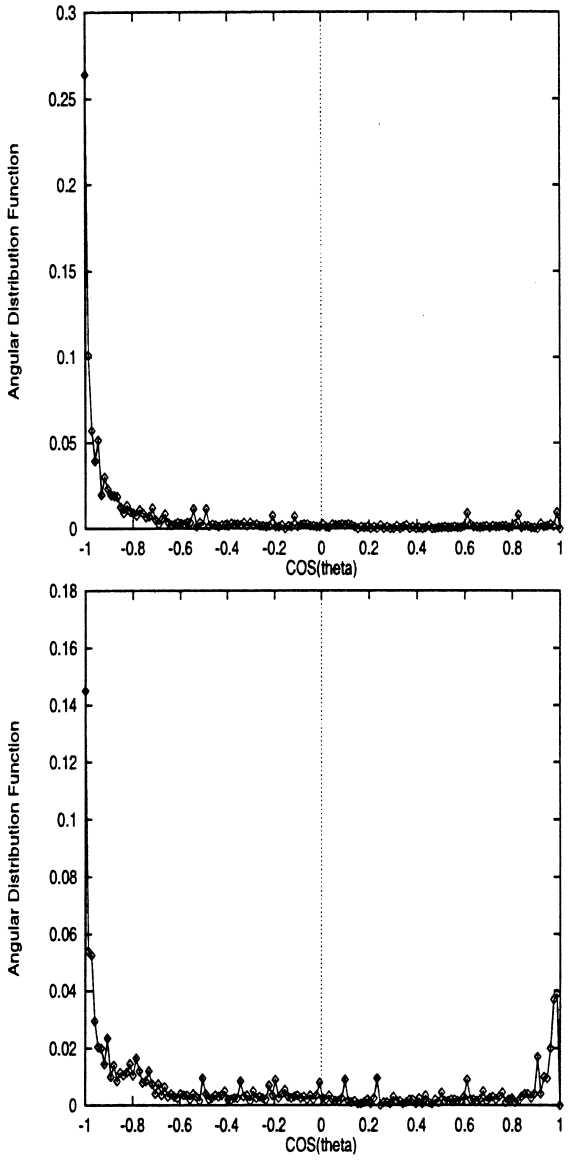

Fig. 3. The angular distribution functions (normalized to 1) are shown for the period from $t = 30{,}000$ to 40,000 in the right figure and for that from $t = 30{,}000$ to 40,000 in the left.

larger than that of the most right particles from the right wall, the melting starts at the left low corner and propagates to adjacent particles. After that, the positions and the tilting angles become more and more random due to the strong wake interaction among fluid and particles. The initially collective oscillation turns to individual particle oscillation which may have a different direction for each particle. The rotation of particle no. 7 as a function of time is plotted in Fig. 2. It oscillates around 180°. The oscillation is directly associated with vortex shedding which has been analyzed by Huang et al. (1994). After the particles become more random, the global angle is not meaningful and an angular distribution function (ADF) should be adopted to statistically describe the particle rotation. The ADF is defined as a probability of finding a single rectangular particle with a given titling angle θ per unit angle and written as

$$f(\theta) = \frac{1}{n}\sum_i \langle \delta(\theta) - \delta(\theta_i) \rangle \tag{23}$$

where δ is Dirac delta function, $\langle \cdots \rangle$ stands for an ensemble average and n is the total number of the particles.

The ensemble average of the angles is carried out for 50 configurations, each 200 time steps apart. The results for the periods from $t = 20{,}000$ to 30,000 and from $t = 30{,}000$ to 40,000 are shown in Fig. 3. It is clearly observed that the long bodies of the rectangular particles broadside on are always dominated during settling as shown in Figs. 1 and 3. The probability is 26% at $\theta = 180°$ for the period from $t = 20{,}000$ to 30,000, and 14% at $\theta = 180°$ and 4% at $\theta = 0°$ for the period from $t = 30{,}000$ to 40,000 as shown in Fig. 3, indicating the horizontal

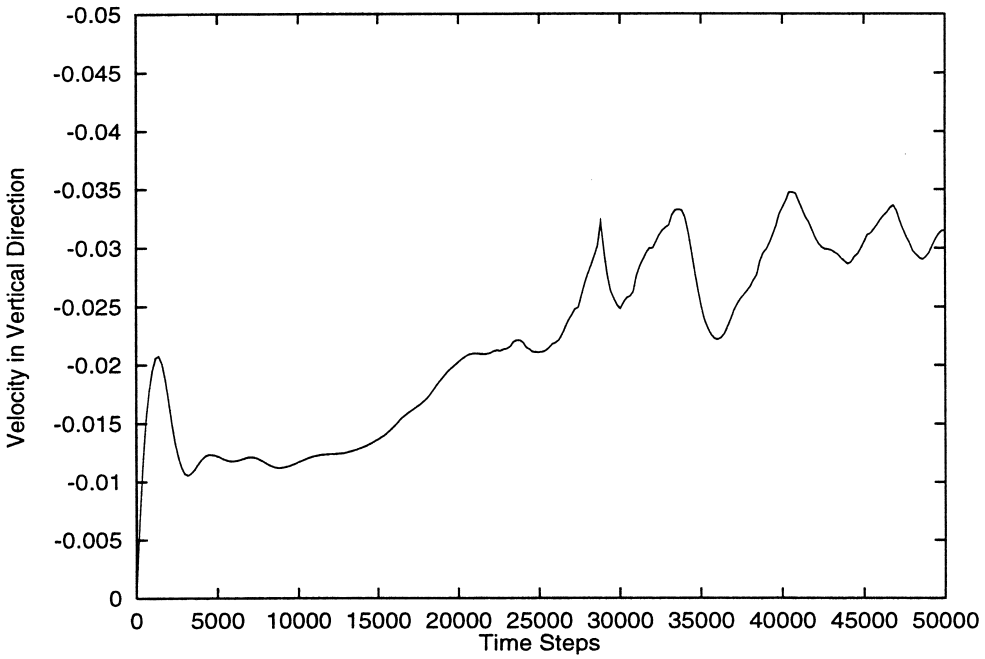

Fig. 4. The global velocity in the settling direction as a function of time.

angle ordering is a feature of slender body in sedimenting flows. The high pressure is produced in the front side of a particle and a wake is generated on the back. The high pressure at the stagnation points gives rise to a couple causing the body to turn broadside on. This has been explained clearly by Joseph et al. (1987) and Huang et al. (1994).

4.2. Structure of clusters

Fig. 4 shows that the global average velocity of all particles in the settling direction is oscillated around 0.03. The final global particle Reynolds number defined by $Re = lu/\nu$ is

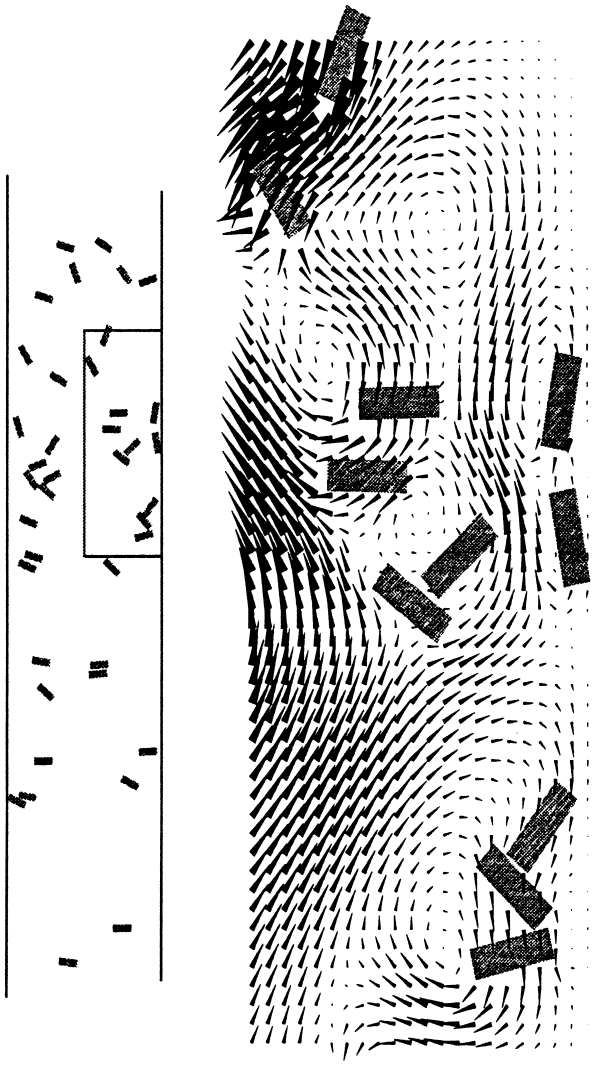

Fig. 5. The velocity field in a part of simulation box at $t = 40{,}000$. The image on the right is a magnified section of the rectangle on the left diagram.

about 18.0 in this simulation. A complex velocity field in a part of the simulation box at $t =$ 40,000 is shown in Fig. 5. As expected, there are many vortex wakes behind rectangular particles or clusters.

One particle may be sucked into the wake of the other particles. A variety type of clusters are observed. The inverted T formed by two particles, stable doublets, triplets are shown in the circles of Fig. 1. The large clusters formed by an array of a few rectangles floating broadside on are shown within the large rectangle in Figs. 1 and 6. Drafting, kissing, and tumbling are originally used to characterize nonlinear interaction between two particles. The mechanisms may be still applicable to multi-particle interaction. One particle or a cluster may draft and kiss to other particle or cluster as shown in Fig. 6 due to strong wake effects and become a large cluster, which is relatively stable for a while. After the cluster sucks the other particle or other cluster, the strength of the wake reduces and some particles in the cluster may be melted. The three particle configurations from the left to the right correspond to a time order of $t = 40{,}000$, 42,000 and 45,000 in Fig. 6, and the walls are not shown here. Three large rectangles at the top of the graph show that two particles are drafting and kissing to a cluster of four particles and become a larger cluster of six particles, then it is melted and divided into two clusters. The

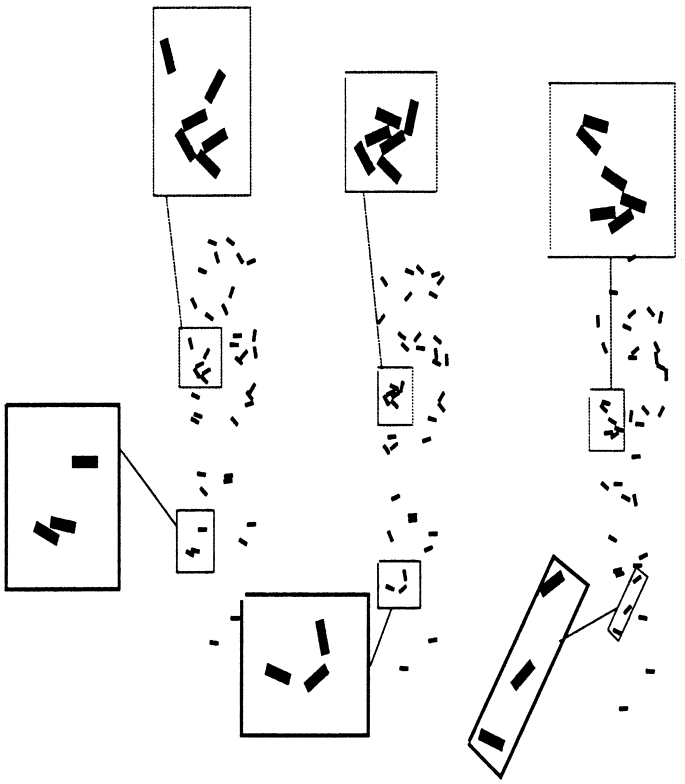

Fig. 6. Drafting, kissing and melting of particle or clusters. The particle configurations from the left to the right correspond to $t = 35{,}000$, 42,000 and 45,000.

particles in three large rectangles at the bottom of the same figure are drafting, kissing and melting.

Therefore, drafting, kissing and melting may be used to characterize the behavior of aggregation and dispersion due to multi-particle interaction governed by inertia-wake effects. These simulation results are well consistent with the experimental work of Joseph et al. (1987) who found the similar behavior of non-spherical particles.

An extension of this simulation to 3D cylinders has been conducted. The results will be reported in another article by Qi (1999). It is shown that the LB method can handle the non-spherical particles correctly. The simulations can provide all dynamical information, such as positions and velocities of solid particles and the velocity field of the fluid. Therefore, micro-structure of particles can be analyzed from the information easily. It is expected that fundamental understanding for aggregation and dispersion of non-spherical particles will be extracted. Today, simulations of non-spherical particles are not a dream any more. This is just a beginning, more exciting works are waiting for us.

5. Conclusions

Fluidization with 40 rectangular particles falling under gravity has been simulated by using the lattice-Boltzmann method. The simulation results show that long bodies of particles turn horizontal dominantly during falling. The inverted T cluster is formed by two rectangles due to the strong wake behind a particle. A variety of clusters, such as doublets, triplets and large clusters formed by an array of a few rectangles, floating broadside on are also found. These behaviors dominated by the effects of inertia are well consistent with the experimental work of Joseph.

Acknowledgements

Author is grateful to Professors D. Joseph and A.J.C. Ladd for their valuable suggestion and encouragement during the course of developing this research program at the Western Michigan University.

References

Aidun, C.K., Lu, Y., 1995. Lattice-Boltzmann simulation of solid suspensions with impermeable boundaries. J. Stat. Phys. 81, 49–61.

Aidun, C.K., Lu, Y., Ding, E., 1998. Direct analysis of particulate suspensions with inertia using the discrete Boltzmann equation. J. Fluid Mech. 373, 287–311.

Aidun, C.K., Qi, D., 1998. A new method for analysis of the fluid interaction with a deformable membrane. J. Stat. Phys. 90, 145–158.

Dahlburg, J.P., Montgomery, D., Doolen, G., 1987. Noise and compressibility in lattice-gas fluids. Phys. Rev. A 36, 2471–2475.

D'Humieres, D., Lallemand, P., Frish, U., 1986. Lattice gas model for 3D hydrodynamics. Europhys. Lett. 2, 291–297.

D'Humieres, D., Lallemand, P., 1987. Numerical simulation of hydrodynamics with lattice gas automata in two dimension. Complex Systems 1, 599–632.

Feng, J., Hu, H.H., Joseph, D.D., 1994a. Direct simulation of initial value problems for the motion of solid bodies in a Newtonian fluid. Part I: sedimentation. J. Fluid Mech. 261, 95–134.

Frich, U., D'Humieres, D., Hasslacher, B., Lallemand, P., Pomeau, Y., Rivet, J.-P., 1987. Lattice gas hydrodynamics in two and three dimensions. Complex Systems 1, 64.

Happel, J., Pfeffer, R., 1960. The motion of two spheres following each other in a viscous fluid. A.I.Ch.E. Journal 6 (1), 129–133.

Hou, S., 1995. Lattice-Boltzmann method for incompressible viscous flow, Ph.D thesis, Kansaa State University.

Huang, P., Feng, J., Joseph, D., 1994. The turning couples on an elliptic particle settling in a vertical channel. J Fluid Mech 271, 1–16.

Joseph, D.D., Fortes, A.F., Lundgreen, T.S., Singh, P., 1987. Nonlinear mechanics of fluidization of beds of spheres cylinders and disks in water. In: Papanicolau, G. (Ed.), Advances in Multiphase Flow and Related Problems, SIAM 101–122.

Koch, D.L., Ladd, A.J.C., 1997. Moderate Reynolds number flows through periodic and random arrays of aligned cylinders. J. Fluid Mech. 349, 31–66.

Ladd, A.J.C., 1994a. Numerical simulations of particulate suspensions via a discretized Boltzmann equation. Part I: theoretical foundation. J. Fluid Mech. 271, 285–309.

Ladd, A.J.C., 1994b. Numerical simulations of particulate suspensions via a discretized Boltzmann equation. Part II: numerical results. J. Fluid Mech. 271, 311–339.

Liboff, R.L., 1990. Kinetic Theroy. Prentice- Hall, Englewood Cliff, NJ.

McNamara, G., Zanetti, G., 1988. Use of Boltzmann equation to simulate lattice-gas automata. Phys. Rev. Lett. 61, 2332–2335.

Qi, D.W., 1997a. Non-spheric colloidal suspensions in three-dimensional space. Int. J. Mod. Phys. C 80, 985–997.

Qi, D.W., 1997b. Computer simulation of coating suspensions. In: Proceedings of Tappi Advanced Coating Fundamental Symposium, Philadelphia, PA, pp. 201–211.

Qi, D.W., 1999a. Lattice-Boltzmann simulations on nonspherical particles in non-zero Reynolds number flows. J Fluid Mech. 385, 41–62.

Qi, D.W., 1999b. Simulations of sedimentation of cylindrical multi-particles in a three-dimensional space. Int. J Multiphase Flows, accepted.

Qian, Y., D'Humieres, D., Lallemand, P., 1992. Lattice BGK models for Navier–Stokes equation. Europhys. Lett. 17, 479–484.

Swope, W.C., Anderson, H.C., Berens, P.H., Wilson, K.R., 1982. A computer simulation method for the calculation of equilibrium constants for formation of physical clusters of molecules: application to small water clusters J. Chem. Phys. 76, 637–649.

Wolfram, S., 1986. Cellular automaton fluids I: Basic theory. J. Stat. Phys. 45, 471–526.